



Introducing KI as a functional electrolyte additive to stabilize Li metal anode

Dequan Huang^a, Cuihong Zeng^a, Menghao Liu^a, Xiaorong Chen^a, Yahao Li^{a,b,*}, Sijiang Hu^{a,*}, Qichang Pan^a, Fenghua Zheng^a, Qingyu Li^a, Hongqiang Wang^{a,*}

^a Guangxi Key Laboratory of Low Carbon Energy Materials, Guangxi New Energy Ship Battery Engineering Technology Research Center, Guangxi Scientific and Technological Achievements Transformation Pilot Research Base of Electrochemical Energy Materials and Devices, School of Chemistry and Pharmaceutical Sciences, Guangxi Normal University, Guilin 541004, China

^b Hubei Provincial Collaborative Innovation Center for New Energy Microgrid, College of Electrical Engineering & New Energy, China Three Gorges University, Yichang, Hubei 443002, China

ARTICLE INFO

Keywords:

Lithium metal anode
Lithium dendrites
Inactive lithium
K⁺ shielding effect
Iodine redox

ABSTRACT

A lithium metal battery (LMBs) is an excellent battery system for advanced electrochemical energy storage. However, the growth of lithium dendrites, the accumulation of inactive lithium, and the side reactions between lithium metal and electrolytes limit the cycling stability of LMBs. Herein, we introduce KI additive into lithium bis(trifluoromethanesulfonyl)imide (LiTFSI)/ether-based electrolyte and lithium hexafluorophosphate (LiPF₆)/ester-based electrolyte for cycling stability improvement of LMBs. Cu-mesh@Ag||Li half-cell with 0.01 M KI additive exhibits a Coulombic efficiency as high as 98.8 % over 200 cycles. The improved performance due to the electrostatic shielding effect formed by K⁺ at low concentration and the rapid recovery of inactive lithium by iodine redox. The corresponding Li||Li symmetrical cell shows an outstanding lifespan of 1400 h at 1.0 mA cm⁻² with 1.0 mAh cm⁻². Meanwhile, in the 1 M LiTFSI + 0.01 M KI electrolyte, the Cu-mesh@Ag-Li||LiFePO₄ (LFP) full cell holds capacity retention of 91.7 % over 800 cycles at 2.0 C, the Li||LiNi_{0.8}Co_{0.1}Mn_{0.1}O₂ (NCM811) full cell possesses much better capacity retention of 54 % after 500 cycles at 1.0 C. This work offers a cost-effective proposal to improve application potential with the electrolyte engineering of rechargeable Li metal batteries.

1. Introduction

As the development and application of new energy cars, new energy ships, and portable electronics are blooming, the market for advanced battery systems with high energy density, long cruising range, and enhanced safety performance has grown ever larger [1–3]. However, traditional lithium-ion batteries can hardly fulfill these high demands for battery systems [4]. On the other hand, lithium metal has a high theoretical specific capacity (3860 mAh g⁻¹) and low electrode potential (−3.04 V vs SHE), which is a promising anode material for next-generation batteries [5–7]. However, the high reactivity of Li results in severe interfacial side reactions, electrolyte consumption, and unstable solid electrolyte interphases (SEI) [8–10]. Besides, uneven Li deposition leads to dendrite growth and inactive lithium accumulation, resulting the rapid capacity fading and safety hazards [11]. Various

strategies, including constructing artificial solid electrolyte interphases [12,13], designing lithiophilic 3D network frameworks as “hosts” [14–16], using high-concentration electrolytes [17] or localized high-concentration electrolytes [18] and developing novel electrolytes [19] for Li metal anode, have been proposed to address these issues.

Electrolyte engineering is a promising approach that reduces interfacial side reactions, suppresses Li dendrite growth, and improves the cycling performance of Li metal batteries [20–23]. Novel electrolyte formulations change the solvation environment of Li-ion and enable uniform Li deposition [24]. Many design strategies have been reported, such as electrolyte additives, new lithium salts, and new solvents [25–27]. Ma and his co-workers used tris (4-fluorophenyl) phosphine (TFPP) as the electrolyte additive to construct a Li₂CO₃/LiF-rich heterostructured SEI, which can realize uniform and stable Li deposition [28]. Cui and his team created inorganic-rich SEI on Li metal by changing the

* Corresponding authors at: Guangxi Key Laboratory of Low Carbon Energy Materials, Guangxi New Energy Ship Battery Engineering Technology Research Center, Guangxi Scientific and Technological Achievements Transformation Pilot Research Base of Electrochemical Energy Materials and Devices, School of Chemistry and Pharmaceutical Sciences, Guangxi Normal University, Guilin 541004, China.

E-mail addresses: liyaha066@126.com (Y. Li), sjhu@gxnu.edu.cn (S. Hu), whq74@gxnu.edu.cn (H. Wang).

<https://doi.org/10.1016/j.cej.2022.140395>

Received 28 August 2022; Received in revised form 25 October 2022; Accepted 13 November 2022

Available online 17 November 2022

1385-8947/© 2022 Elsevier B.V. All rights reserved.

Li^+ solvation environment. This strategy improved the Coulombic efficiency and achieved extended cycle life of the anode-free cell [29]. Although these strategies endue Li metal batteries with long cycle life, electrolyte additives are continuously consumed during cycling and eventually lose their effect [30]. In addition, the accumulation of inactive lithium is inevitable during the cycling process. Modifications are required further to improve cyclability and cost efficiency [31].

In this work, we reported the positive effect of KI as an electrolyte additive on the uniform Li plating/stripping on a Cu-mesh@Ag substrate. An iodine redox can effectively recover inactive Li in dendrites, and Li fragments from electrochemically uneven lithium deposition [31]. Simultaneously, reversible I^-/I_3^- redox can be achieved when the discharge voltage of the cathode exceeds 2.89 V, enabling the recovery of inactive lithium back to the cathode [32]. In addition, it was demonstrated that during the Li plating process, K^+ ions are electrostatically adsorbed on the anode surface, which could regulate Li deposition behavior and inhibit the dendrite growth (Fig. 1). The resultant Cu-mesh@Ag||Li half-cell achieves a high Coulombic efficiency (98.8 % over 200 cycles), and the symmetrical cell exhibits an ultralong lifespan (~1400 h). When coupled with cathodes like LiFePO_4 and $\text{LiNi}_{0.8}\text{Co}_{0.1}\text{Mn}_{0.1}\text{O}_2$, the cells showed considerable cyclability and excellent rate performance.

2. Experimental section

2.1. Materials

The Li foil was purchased from China Energy Lithium Co., Ltd. The lithium salts lithium bis(trifluoromethyl)sulfonamide (LiTFSI), lithium hexafluorophosphate (LiPF_6) and the solvents 1,3-dioxolane (DOL), 1,2-dimethoxyethane (DME), ethylene carbonate (EC), dimethyl carbonate (DMC) were purchased from Macklin (Shanghai, China). The additive, potassium iodide (KI), was purchased from Aladdin (Shanghai, China). All the reagents were stored and prepared inside an argon-filled glove

box with monitored H_2O and O_2 concentrations.

2.2. Preparation of Cu-mesh@Ag

The commercial Cu-mesh was cut into 12 mm diameter discs, then washed with a degreasing solution at 60 °C for 20 min. The residual liquid was cleaned with deionized water. The Cu-mesh was sensitized with 10 wt% HCl for 5 min, then washed and dried at 80 °C for 24 h to obtain a pretreated Cu-mesh. An electroless deposition solution consisting of AgNO_3 , sodium potassium tartrate, and disodium ethylenediaminetetraacetic acid was used. The Cu-mesh was electroless plated in the solution for 30 s and then washed and dried at 80 °C for 24 h to obtain Cu-mesh@Ag.

2.3. Preparation of electrolyte

1 M LiTFSI dissolved in DOL and DME (1:1 by volume) without any additive was selected as the fundamental electrolyte, denoted as 1 M LiTFSI. Specifically, 1 M LiTFSI electrolyte was prepared by 2.87 g LiTFSI dissolving in 5 mL DME + 5 mL DOL.

The KI-containing electrolyte was prepared by adding 0.005 M (0.0083 g), 0.01 M (0.0166 g), and 0.02 M KI (0.0332 g) additives into the fundamental electrolyte, marked as 1 M LiTFSI + 0.005 M KI, 1 M LiTFSI + 0.01 M KI, 1 M LiTFSI + 0.02 M KI, respectively. A digital image of the color evolution (Fig. S1) shows that with the introduction of KI additives, the color of the electrolyte changes to yellow, indicating that KI can dissolve in the electrolyte. In the Li||NCM811 full cells, 1 M LiPF_6 dissolved in EC and DMC (1:1 by volume) without any additive was selected as the fundamental electrolyte, named 1 M LiPF_6 . 1 M LiPF_6 electrolyte was prepared by 1.52 g LiPF_6 dissolving in 5 mL EC + 5 mL DMC. The KI-containing electrolyte was prepared by adding 0.005 M (0.0083 g) and 0.01 M KI (0.0166 g) into the fundamental electrolyte, designated as 1 M LiPF_6 + 0.005 M KI, 1 M LiPF_6 + 0.01 M KI, respectively.

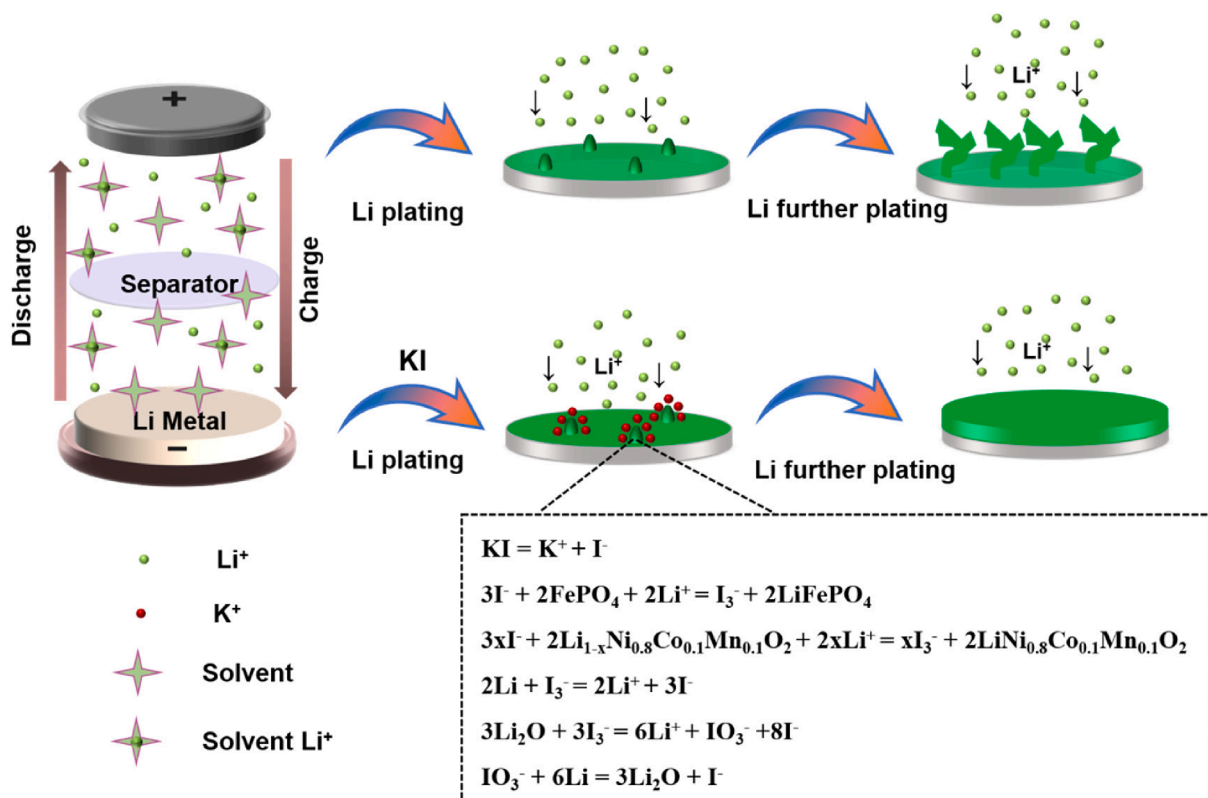


Fig. 1. Schematics of the Li deposition behavior in 1 M LiTFSI with and without 0.01 M KI electrolytes.

2.4. Characterization

The morphology was obtained with a scanning electron microscope (SEM, FEI Quanta 200 FEG), the field voltage was 30 kV, and the resolution was 3.0 nm. The X-ray photoelectron spectroscopy (XPS, ESCALab220i-XL) with 300 W Al K α radiations was carried out to detect the chemical composition of the SEI layer. In-situ Raman spectra spectroscopy (Renishaw in Via Quotation) was used to explore the Li plating/stripping behavior. The Raman tests were carried out at room temperature using a 785 nm laser, with the cells plating/stripping at a current density of 0.25 mA cm⁻² with a capacity of 0.5 mAh cm⁻².

2.5. DFT calculation method

The DFT calculation was applied to calculate the HOMO and LUMO energy of LiPF₆, LiTFSI, EC, DMC, DME, DOL, and I₃⁻ using B3LYP in Gaussian 09, molecular geometry optimized by basis sets for 6-31+g (d, p).

2.6. Electrochemical measurements

CR2032-type coin cells were assembled in a glove box filled with argon using Cu-mesh@Ag, lithium foil, and Celgard 2400 diaphragm as the working electrode, counter electrode, and membrane, respectively. The amount of electrolyte is 60 mL. The coin cells were tested with a LAND battery testing system. To evaluate the Coulombic efficiency, 1.0 mAh cm⁻² of Li was first deposited on the Cu-mesh@Ag current collector and then stripped to a cutoff voltage of 3.0 V at 1.0 mA cm⁻², Coulombic efficiency equals the quotient of stripping capacity and plating capacity for each cycle. To evaluate the surface morphology of lithium deposition, the Cu-mesh@Ag current collector was first plated with 1.0, 3.0, 5.0, and 8.0 mAh cm⁻² of Li at 0.1 mA cm⁻², respectively. The micromorphology of the samples were analyzed by SEM. The Li foil was assembled into a symmetrical cell to evaluate the cycling stability of different electrolytes. These symmetrical cells were cycled at 1 mA cm⁻² and 1 mA cm⁻². The electrochemical impedance spectroscopy (EIS) tests were carried out using an IM6 electrochemical workstation with a frequency range of 100 kHz to 0.01 Hz and an amplitude of 5 mV. The Cu-mesh@Ag current collector plated with 3.0 mAh cm⁻² of Li was paired with LiFePO₄ (LFP) cathode to assemble a full battery, denoted as Cu-mesh@Ag-Li||LFP, which was measured between 2.5 ~ 4 V and Li||NCM was measured between 2.7 ~ 4.3 V at different current densities, respectively.

3. Results and discussion

3.1. Choice of lithium deposition substrate

The cyclic stability of Cu foil, Cu-mesh, and Cu-mesh@Ag during Li plating/stripping was firstly investigated to find the best substrate for later tests. As shown in Fig. S2, the Coulombic efficiency of Cu and Cu-mesh substrates show a significant decrease after 100 cycles, while the Coulombic efficiency of Cu-mesh@Ag substrate still exceeds 98 % after 150 cycles. Therefore, the Cu-mesh@Ag is a more suitable substrate, and all subsequent studies are carried out using the Cu-mesh@Ag host.

3.2. Electrochemical properties

To evaluate the reversibility of Li plating/stripping process, the Coulombic efficiency of Cu-mesh@Ag||Li half cells with various electrolytes was monitored. For the fundamental electrolyte (1 M LiTFSI), the Coulombic efficiency is around 98.5 % in the first 100 cycles and gradually decreases to 69.4 % after 165 cycles (Fig. 2a). The rapid capacity fading may be due to the dendrite growth and inactive lithium accumulation. For the 1 M LiTFSI + 0.005 M KI electrolyte, the Coulombic efficiency is around 98.5 % in the first 120 cycles, which then

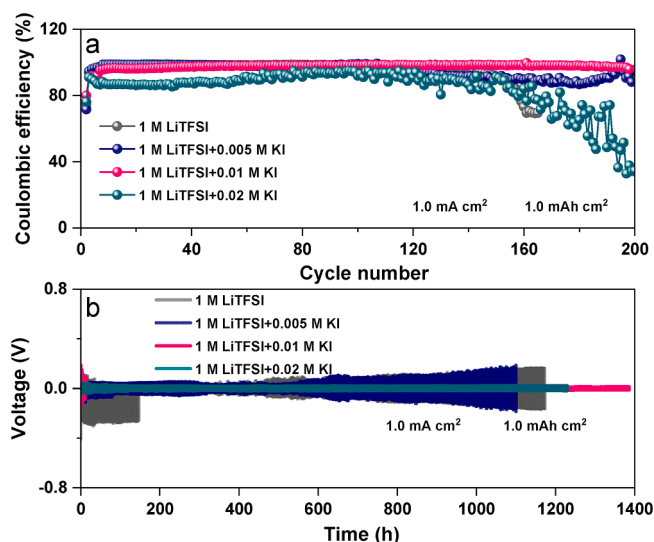


Fig. 2. (a) Coulombic efficiency and of Cu-mesh@Ag||Li half cells at 1.0 mA cm⁻² and 1.0 mAh cm⁻² in different electrolytes, (b) Cycling stability of Li||Li symmetrical cells in different electrolytes at 1.0 mA cm⁻² and 1.0 mAh cm⁻².

moves between 87 and 97 % in the subsequent 80 cycles and exhibits 88.6 % capacity retention after 200 cycles. This result reveals that the introduction of KI contributes to the improvement of cycle life. Inspiringly, it can be observed that the cell with the 1 M LiTFSI + 0.01 M KI electrolyte maintains a stable Coulombic efficiency of 98.5 % over 200 cycles. These results validate that the KI additive can effectively suppress the dendrite growth and eliminate inactive lithium. But for the 1 M LiTFSI + 0.02 M KI electrolyte, the Coulombic efficiency fluctuates between 86 and 94 % in the initial 160 cycles, and the capacity retention reduced to 34.6 % after 200 cycles. It may be ascribed to the excessive I⁻ content that eliminates active lithium and results in lower Coulombic efficiency.

The electrostatic shielding effect of K⁺ and I⁻/I₃⁻ redox processes are schematically illustrated in Fig. 1. In the initial stage of lithium deposition, due to the fluctuation of the electric field, Li deposits on the electrode and unavoidably forms some tips. The protruding tip shows a stronger electric field, leading to the preferential deposition of Li⁺ in the tip [30,33,34]. The continuous amplification of the tips eventually leads to the formation of Li dendrites. When the KI additive was introduced, the K⁺ at an appropriate concentration can offer a self-healing charge shielding effect that can effectively suppress the continuous deposition of Li ions at the tip, thereby inhibiting the dendrite growth. On the other hand, the reversible I⁻/I₃⁻ redox processes can effectively eliminate the grown Li dendrites (dead Li). It is worth noting that in the same electrolyte environment, a unique charge shielding effect occurs when the actual reduction potential of K⁺ is lower than that of Li⁺. Therefore, the actual reduction potentials of K⁺ and Li⁺ at different concentrations were calculated according to the Nernst equation [33,34]. As shown in Table S1, the standard reduction potentials of K/K⁺ and Li/Li⁺ were -2.93 V and -3.04 V vs SHE, respectively. When the K⁺ concentrations were 0.005 M and 0.01 M, the effective reduction potentials were -3.067 and -3.049 V vs SHE, respectively. The effective reduction potential of K/K⁺ at low concentration is lower than Li/Li⁺. Therefore, K⁺ electrodeposition does not occur in 1 M LiTFSI + 0.005 M KI and 1 M LiTFSI + 0.01 M KI electrolytes. When the K⁺ concentration was increased to 0.02 M, the effective reduction potential of K/K⁺ (-3.032 V vs SHE) was higher than that of Li/Li⁺, which caused K⁺ to lose its self-healing charge shielding effect and resulted in lower Coulombic efficiency. At 2.0 mA cm⁻² and 1.0 mAh cm⁻², the Coulombic efficiency is as high as 97.1 % over 125 cycles (Fig. S3) in 1 M LiTFSI + 0.01 M KI electrolyte. In contrast, the Coulombic efficiency values show apparent attenuation to 80.5 %, 89.7 %, and 84.9 % after 125 cycles in the 1 M

LiTFSI, 1 M LiTFSI + 0.005 M KI, and 1 M LiTFSI + 0.02 M KI electrolytes, respectively. In addition, the voltage profiles of Li plating/stripping process as shown in Fig. S4a and 4b, Cu-mesh@Ag||Li half cells with 1 M LiTFSI + 0.01 M KI electrolyte exhibited a higher deposition potential and lower polarization potential than 1 M LiTFSI electrolyte, indicating a lower energy barrier for lithium deposition and its favorable Li stripping/plating process. Therefore, with an appropriate amount of KI additives, K^+ electrostatic shield can be formed on the predeposited Li tips, repelling subsequent Li^+ to the reach of the Li-free tip. As a result, uniform Li deposition was achieved, and the cycle stability of Li metal anodes were improved.

Furthermore, the cycling performance of symmetrical Li||Li cells in various electrolytes was investigated. Fig. 2b shows the Li plating/stripping profiles at 1.0 mA cm^{-2} and 1.0 mAh cm^{-2} . We can see that the cell with the 1 M LiTFSI + 0.01 M KI electrolyte exhibits stable cycling with a hysteresis voltage of about 13 mV for over 1400 h. Note that the overpotentials in the first 30 h were larger than in the regular cycles. It was due to the noncomplete activation of the testing battery, resulting in the polarization voltage exceeding regular cycling. Meanwhile, the overpotential of cells with the 1 M LiTFSI and 1 M LiTFSI + 0.005 M KI electrolytes show irregular fluctuations. The overpotential increase to about 170 mV after 1100 h, implying the unstable electrode/electrolyte interface, which results from dendrite growth and inactive Li accumulation. Surprisingly, the cell with the 1 M LiTFSI + 0.02 M KI electrolyte also exhibited stable cycling and an overpotential of about 30 mV for over 1200 h. It may be ascribed to the abundant lithium content in Li||Li symmetrical cell. The excessive I^- content can effectively eliminate inactive lithium without negatively affecting active lithium, resulting in better cycling performance than the cells with 1 M LiTFSI and 1 M LiTFSI + 0.005 M KI electrolytes. Thus, the stable cycling performance and low overpotential indicate that 0.01 M is the optimal amount for KI addition, with which the Li plating/stripping process is effectively enhanced.

The long-term cycling stability of the Cu-mesh@Ag electrode in different electrolytes was tested in Cu-mesh@Ag-Li||Cu-mesh@Ag-Li symmetric cell. Firstly, 5.0 mAh cm^{-2} of Li were deposited on Cu-mesh@Ag substrates at 0.1 mA cm^{-2} to obtain a Cu-mesh@Ag-Li electrode, assembled into a symmetric cell tested at 1.0 mA cm^{-2} and 1.0 mAh cm^{-2} for a constant-current long-cycle test. As shown in Fig. S5, the Cu-mesh@Ag-Li||Cu-mesh@Ag-Li symmetrical cell exhibits severe voltage fluctuations and high voltage hysteresis (even larger than 150 mV) in 1 M LiTFSI electrolyte, which due to uncontrollable dendrite growth, unstable SEI, and the accumulation of inactive lithium. In contrast, for the cell with 1 M LiTFSI + 0.01 M KI electrolyte, the symmetrical cell exhibits a smaller and relatively stable polarization potential for more than 700 h, and there is no noticeable voltage fluctuation. This significant difference further indicates that stable Li plating/stripping, low polarization, and excellent stability have been achieved in electrolytes with 0.01 M KI additive. The superb stability is attributed to the rapid recovery of inactive lithium by the I^-/I_3^- redox. At the same time, the non-redox K^+ can spontaneously adsorb on the dendrite tip to form a charge shield, which effectively inhibits the dendrite growth and the inactive lithium accumulation.

The Li metal plating behavior on the Cu-mesh@Ag substrate in different electrolytes and deposition capacities were investigated. For the cells at 0.1 mA cm^{-2} and 1.0 mAh cm^{-2} (Fig. 3a, e), no apparent dendrite structure can be seen owing to the small Li deposition amount. There has a similar dendrites structure (marked in red circle) on the surface in 1 M LiTFSI electrolyte (Fig. 3a), and no apparent Li dendrite was found on the surface in 1 M LiTFSI + 0.01 M KI electrolyte (Fig. 3e). With the Li deposition capacity increased to 3.0 and 5.0 mAh cm^{-2} , abundant Li dendrites were formed on Cu-mesh@Ag substrate with 1 M LiTFSI fundamental electrolyte (Fig. 3b, c). In contrast, the cell with the 1 M LiTFSI + 0.01 M KI electrolyte shows almost no Li dendrites under the same deposition condition. Notably, the cell with 1 M LiTFSI + 0.01 M KI electrolyte exhibited a uniform and smooth deposition morphology

in the substrate. No dendrite tips were seen, which proves the charge shielding effect of K^+ effectively suppresses the growth of dendrites. As the deposition capacity continues to increase to 8.0 mAh cm^{-2} , larger dendrites can be seen on the substrate surface in the 1 M LiTFSI electrolyte. In contrast, dense Li deposition morphology is exhibited in the 1 M LiTFSI + 0.01 M KI electrolyte. It indicates that a small amount of KI additive can effectively promote smooth Li deposition while significantly inhibiting dendrite growth. At the same time, reducing I^- can effectively clean the inactive lithium, so it has a uniform and smooth deposition morphology.

To in-depth understand the reaction, *in operando* Raman measurements were performed. The *in operando* Raman spectra are shown in Fig. 3i-l. There was no characteristic peak of I_3^- in the 1 M LiTFSI electrolyte (Fig. 3k-l). The pronounced peaks at 289, 418, 743, and 1150 cm^{-1} represent the stretching modes of TFSI $^-$ [35]. At the same time, other peaks at 880 and 950 cm^{-1} represent the stretching modes of DME and DOL, respectively [36]. In contrast, an obvious characteristic peak appeared at about 118 cm^{-1} and gradually intensified during the Li plating in 1 M LiTFSI + 0.01 M KI electrolyte (Fig. 3i-j). This peak can be attributed to the symmetric stretching mode of I_3^- , corresponding to the conversion of I^- to I_3^- [32,37,38]. As the stripping process begins, the disappearing peaks indicate the reaction transition from I_3^- to I^- . The subsequent enhancement of the I_3^- peak suggests the migration of lithium ions to the cathode. In addition, uniform lithium deposition can be seen in 1 M LiTFSI and 1 M LiTFSI + 0.01 M KI electrolytes (Fig. S6). It may be due to the presence of Ag particles in the Cu-mesh@Ag electrode and can guide the homogeneous deposition of Li^+ . However, 1 M LiTFSI + 0.01 M KI electrolyte shows stronger anion and solvent peaks, indicating a more stable electrolyte environment, which is more conducive to the long cycle life of lithium metal batteries. Moreover, the KI additives were introduced into the electrolyte, and the peaks of TFSI $^-$, DME, and DOL did not shift significantly, indicating that KI did not have obvious solvation effects with anions and solvents in the electrolyte. These results suggest that the redox behaviors of iodine can effectively enhance inactive lithium's recovery.

To further understand the effect of KI additives on the composition and structure of SEI, XPS was used to monitor the elemental composition of the SEI layer after 100 cycles. As shown in Fig. 4 and Fig. S7, the elements on the traditional Li metal surface with LiTFSI electrolyte are Li, C, O, N and F. In contrast, the major elements on the Li metal surface with LiTFSI + 0.01 M KI electrolyte are Li, C, O, N, F, and I. In the C1s spectra (Fig. 4a), the peaks at 284.8, 286.5, 288.6, 290, and 293 eV correspond to the C—C, C—O, C=O, Li_2CO_3 , and C—F, respectively. These functional groups mainly came from the decomposition products of DME and DOL [39,40]. It is found that the KI additive can enhance the C—F bond content (Fig. 4a), indicating that the introduction of the KI additive can effectively limit the decomposition of LiTFSI. Even in the fifth cycle, we can also see the enhanced C—F bond content (Figure S7a). The C—F bond is beneficial to the formation of LiF, which can effectively reduce the diffusion barrier of Li^+ in the SEI layer, thereby promoting Li ion transport [11,41]. The peaks at 53.8, 54.5, and 55.6 eV in the Li 1s spectra (Fig. 4b) are related to Li_2O , Li_2CO_3 , and LiF, respectively. And the peaks at 530.4, 530.8, and 531.9 eV in the O 1s spectra (Fig. 4c) are related to Li_2O , C=O, and C—O, respectively [42]. Compared with the a few cycles (Fig. S7b and 7c), we can see the weakened Li_2O species content in 1 M LiTFSI + 0.01 M KI electrolyte after 100 cycles. It proves that reductive iodine can effectively eliminate inactive lithium, including Li_2O , enabling the battery to have a longer cycle. The peaks for C—F (688.9 eV) and LiF (684.8 eV) can be observed in spectra of F 1s (Fig. 4d and Fig. S7d).

In contrast, the SEI film formed in the LiTFSI with KI electrolyte has enhanced LiF peaks and a reduced F—C bond. Significantly improved LiF peaks indicate that TFSI $^-$ anions have participated in forming SEI, and the weakened C—F peak suggests that electrolyte decomposition is suppressed. At the same time, compared with 1 M LiTFSI electrolyte, the SEI composition of 1 M LiTFSI + 0.01 M KI electrolyte also exhibits less

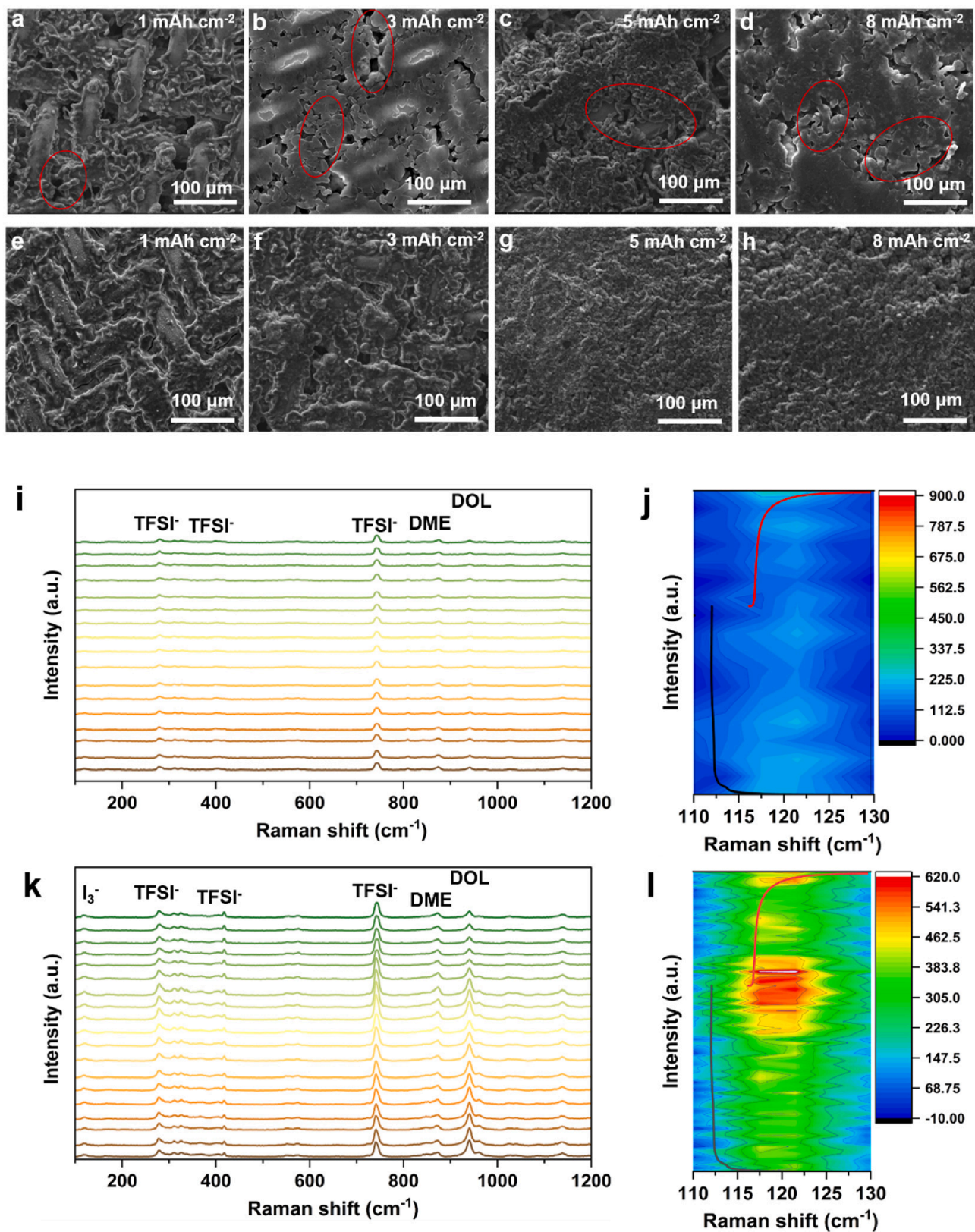


Fig. 3. SEM images of Li deposition morphologies on Cu-mesh@Ag at 0.1 mA cm⁻² and a capacity of 1.0 mAh cm⁻², 3.0 mAh cm⁻², 5.0 mAh cm⁻², 8.0 mAh cm⁻² in LiTFSI electrolytes without (a-d) and with (e-h) KI, respectively; (i) Waterfall diagram of the *in operando* Raman spectra of Cu-mesh@Ag||Li half cells in 1 M LiTFSI electrolyte, (j) The selected local Contour plot of I₃⁻ in 1 M LiTFSI electrolyte, (k) Waterfall diagram of the *in operando* Raman spectra of Cu-mesh@Ag||Li half cells in 1 M LiTFSI + 0.01 M KI electrolytes, (l) The selected local Contour plot of I₃⁻ in 1 M LiTFSI + 0.01 M KI electrolytes.

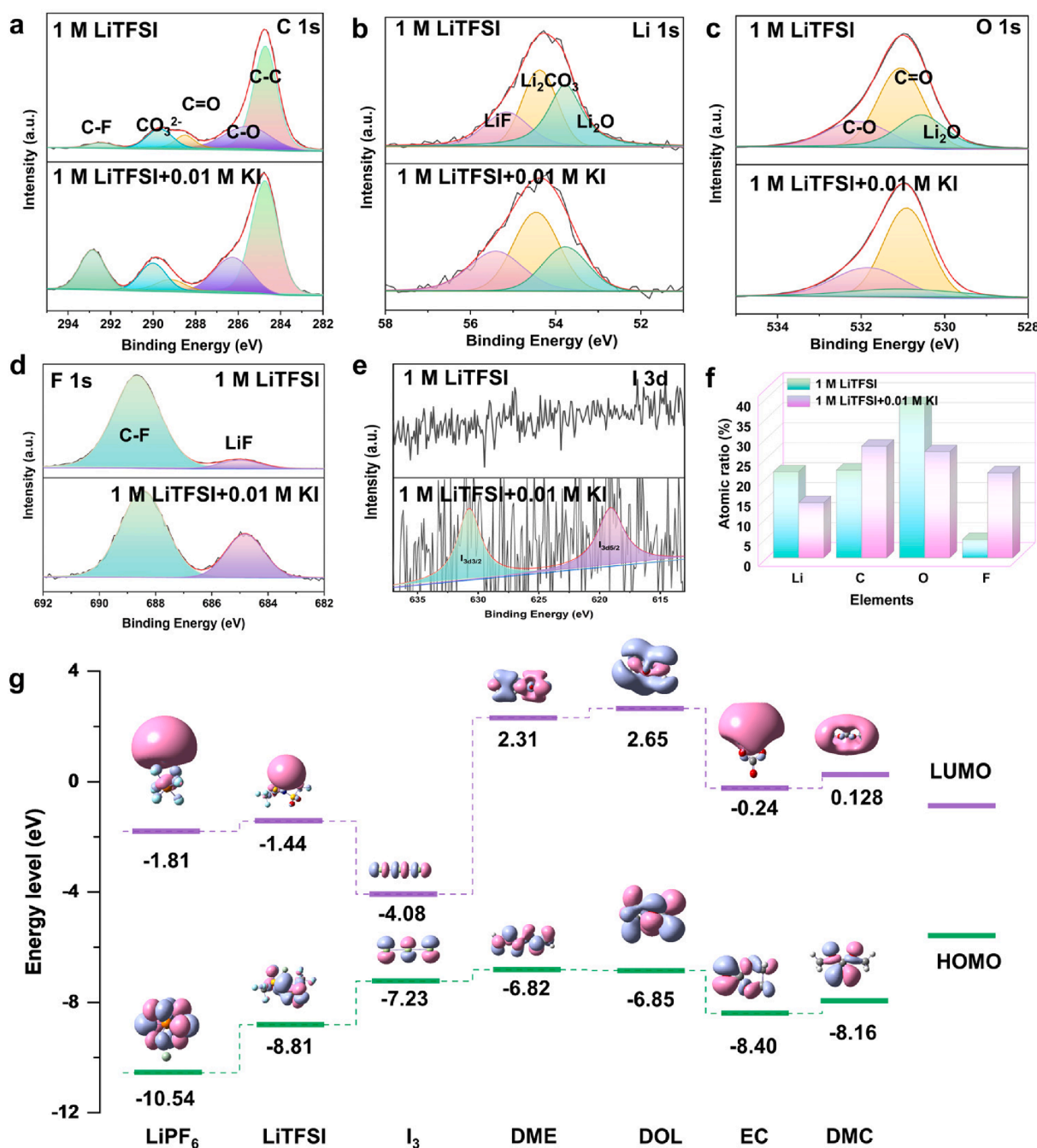


Fig. 4. XPS spectra of (a) C 1s, (b) Li 1s, (c) O 1s, (d) F 1s, (e) I 3d, and (f) the content of the SEI composition after 100 cycles in Li||Cu-mesh@Ag cells in different electrolytes, (g) LUMO-HOMO energy level diagram of the different solutes and solvents.

lithium content (Fig. 4f), indicating the elimination of inactive lithium by Γ^- . Moreover, the I signal (Fig. 4e) is preserved after long-term cycling. Hence, the LiTFSI with KI electrolyte can reduce the Li_2O species in the SEI film and promote the formation of LiF species. Robust and stable SEI film reduces side reactions between metal anode and electrolyte, resulting in improved battery electrochemical performance. According to the frontier molecular orbital theory (Fig. 4g), the lower the LUMO level of the molecule, the more likely it is to accept electrons for reduction reactions during charge and discharge. The I_3^- species have a relatively low LUMO energy level of -4.08 eV. This means a higher electron affinity and easier reduction to I^- during the Li plating process. In other words, compared with other solutes and solvents, I_3^- is easier to react with lithium metal, thereby effectively eliminating the inactive

lithium generated by dendrite accumulation.

To evaluate the electrolyte performance in practical application, we used LFP as the cathode and Cu-mesh@Ag-Li as the anode to assemble full cells and test their electrochemical performance. First, 3.0 mAh cm^{-2} Li was deposited on the Cu-mesh@Ag substrates. Then the Cu-mesh@Ag-Li was paired with LFP cathodes to obtain Cu-mesh@Ag-Li||LFP. The loading mass of LFP is $2.0\text{--}2.5 \text{ mg cm}^{-2}$. Fig. 5a shows the initial charge–discharge profiles of Cu-mesh@Ag-Li||LFP full cells at 0.1 C in 1 M LiTFSI, 1 M LiTFSI + 0.005 M KI , and 1 M LiTFSI + 0.01 M KI electrolytes. The initial discharge capacities are 155.4, 162.7, and 167.1 mAh/g in 1 M LiTFSI, 1 M LiTFSI + 0.005 M KI , and 1 M LiTFSI + 0.01 M KI electrolytes, respectively. Compared to the LFP full cell with no KI additive, significantly improved specific capacities at first charge

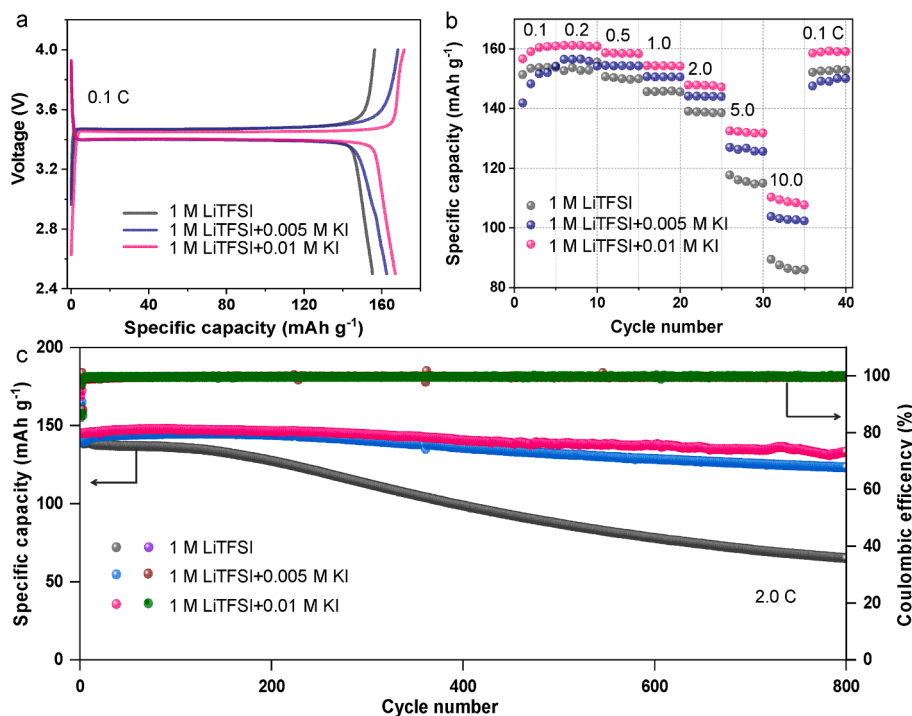


Fig. 5. (a) Initial charge and discharge curve at 0.1 C, (b) Rate performance, (c) Cycling performance and Coulombic efficiency of Cu-mesh@Ag-Li||LFP at 2.0 C in different electrolytes.

and discharge are observed in cells with 1 M LiTFSI + 0.005 M KI and 1 M LiTFSI + 0.01 M KI electrolytes, indicating improved kinetics after KI introduction. The enhanced electrochemical performance of Cu-mesh@Ag-Li||LFP full cell in the 1 M LiTFSI + 0.01 M KI electrolyte can be ascribed to the inhibition of Li dendrites by K^+ and the rapid reversible recovery of batteries by I^- . Fig. 5b shows the rate performances of Cu-mesh@Ag-Li||LFP cells with different electrolytes. The Cu-mesh@Ag-Li||LFP full cell with 0.01 M KI additive shows superior rate performance compared with other cells. The discharge capacities of

Cu-mesh@Ag-Li||LFP full cell with 0.01 M KI at 0.2 and 10.0 C are 161.2 and 108.7 mAh/g, which are higher than the full cells with fundamental electrolyte (discharge capacity of 152.8 mAh/g at 0.2 C and 86.4 mAh/g at 10.0 C) and with 0.005 M KI additive (discharge capacity of 156.5 mAh/g at 0.2 C and 102.8 mAh/g at 10.0 C). Moreover, the cycle performances of Cu-mesh@Ag-Li||LFP full cells are shown in Fig. 5c. At 2.0 C, the initial discharge capacity of Cu-mesh@Ag-Li||LFP with 1 M LiTFSI + 0.01 M KI electrolyte is 145.2 mAh/g, which only reduces to 133.2 mAh/g after 800 cycles (capacity retention 91.7 %), suggest good

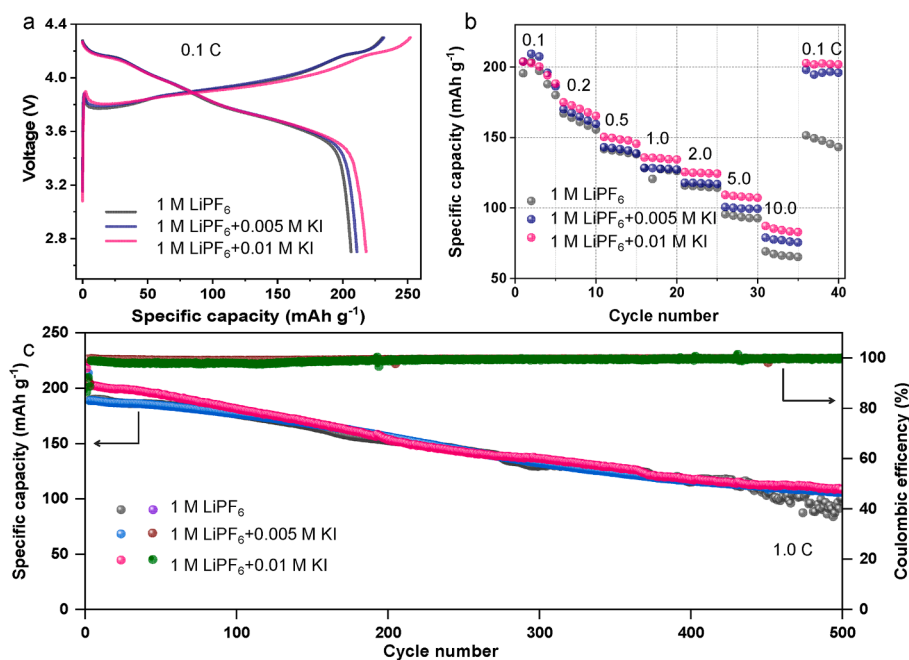


Fig. 6. (a) Initial charge and discharge curve at 0.1 C, (b) Rate performance, (c) Cycling performance and Coulombic efficiency of Li||NCM811 at 1.0 C in different electrolytes.

cycle performance. This is attributed to the redox behavior of iodine that can effectively restore inactive lithium.

The cyclic voltammetry curves of Cu-mesh@Ag-Li||LFP are presented in Fig. S6a. Cu-mesh@Ag-Li||LFP full cell exhibited the smallest potential interval and most substantial redox peaks in 1 M LiTFSI + 0.01 M KI electrolyte, indicating the preeminent redox kinetics. Fig. S6b shows the EIS of Cu-mesh@Ag-Li||LFP in different electrolytes. According to the Nyquist plots, the charge transfer resistance (R_{ct}) values of Cu-mesh@Ag-Li||LFP are 102.2, 248.3, and 518.1 Ω in 1 M LiTFSI, 1 M LiTFSI + 0.005 M KI, and 1 M LiTFSI + 0.01 M KI electrolytes, respectively. Meanwhile, Cu-mesh@Ag-Li||LFP full cell delivers the lowest contact resistance of 2.95 Ω in 1 M LiTFSI + 0.01 M KI electrolyte, lower than 1 M LiTFSI electrolyte (8.16 Ω) and 1 M LiTFSI + 0.005 M KI electrolyte (5.06 Ω), indicating the improved kinetics. The Cu-mesh@Ag-Li||LFP has the smallest impedance in 1 M LiTFSI + 0.01 M KI electrolyte, which is attributed to the presence of K^+ on the current collectors to guide the uniform Li deposition and suppress the lithium dendrite growth. In contrast, the recovery of inactive lithium by reducing iodine reduces the resistance to ion migration simultaneously, so the battery has more excellent performance.

LMB full cells were assembled using NMC811 cathodes, using 1 M LiPF₆ in EC/DMC with different KI additives. Fig. 6a shows the initial discharge capacities of full cells in 1 M LiPF₆, 1 M LiPF₆ + 0.005 M KI, and 1 M LiPF₆ + 0.01 M KI electrolytes are 206.7, 211.2, and 218.2 mAh/g, respectively, indicating the improved kinetics with 1 M LiPF₆ + 0.01 M KI electrolyte. In addition, the cell with 1 M LiPF₆ + 0.01 M KI electrolyte displayed an excellent rate capability, with discharge specific capacities of 170.3 mAh/g at 0.2 C, 124.9 mAh/g at 2.0 C, and 108.5 mAh/g at 5.0 C, thanks to the charge shielding effect of K^+ on the dendrite tip and the rapid recovery of inactive lithium by the I^- redox. More importantly, the discharge capacity recovered to 202.8 mAh/g when the rate returned to 0.1 C. Moreover, it can be seen that the cell with 1 M LiPF₆ + 0.01 M KI electrolyte exhibited excellent cycling performance with specific capacity retaining to 109.4 mAh/g, delivering better capacity retention of 54 % after 500 cycles, with Coulombic efficiency >99.7 % at 1C (Fig. 6c). And the cell of the 1 M LiPF₆ exhibited wildly fluctuating Coulombic efficiency after 430 cycles, indicating an unstable Li plating/stripping process. No extra oxidation peaks exist in the CV curve for Li||NMC811 full cells with different electrolytes (Fig. S7a). However, the larger peak area and stronger peak intensity were exhibited in the 1 M LiPF₆ + 0.01 M KI electrolyte, indicating its fast reaction kinetics in the full cell. At the same time, the smaller charge transfer impedance and interfacial contact impedance (Fig. S7b) also demonstrate the fast reaction kinetics in the Li||NMC811 full cell with 1 M LiPF₆ + 0.01 M KI electrolyte. Collectively, the electrochemical Evaluation results suggest that KI can promote stable cycling of Li||NMC811 full cell and contribute to the formation of stable interfacial layers on both Li metal anode and NMC811 cathode during cycling.

4. Conclusions

The practical improvement in the electrochemical performances of Li metal anode in Cu-mesh@Ag-Li||LFP and Li||NMC811 full cells by introducing optimized amounts (0.01 M) of the KI additives into the LiTFSI/ether-based electrolyte is demonstrated. The electrostatic shield of K^+ can help adjust the electrochemical deposition of Li^+ , improving the cyclic performance of the Li metal anode. Meanwhile, the I^- can rapidly recover inactive lithium due to iodine redox. Uniform and dense Li deposition have been achieved and exhibited a high Coulombic efficiency of 98.8 % over 200 cycles in the 1 M LiTFSI + 0.01 M KI electrolyte. Remarkably, the Cu-mesh@Ag-Li||LFP and Li||NMC811 full cell show superior rate and cycle performances, suggesting their excellent potential in practical application.

Declaration of Competing Interest

The authors declare that they have no known competing financial interests or personal relationships that could have appeared to influence the work reported in this paper.

Data availability

Data will be made available on request.

Acknowledgments

We acknowledge the support from the Guangxi Natural Science Foundation (grant no. 2021GXNSFDA075012), Guangxi Technology Base and Talent Subject (GUIKE AD20297086), National Natural Science Foundation of China (grant no. 22169004, U20A20249), and Innovation Project of Guangxi Graduate Education (JGY2022031).

Appendix A. Supplementary data

Supplementary data to this article can be found online at <https://doi.org/10.1016/j.cej.2022.140395>.

References

- [1] C.-C. Su, M. He, M. Cai, J. Shi, R. Amine, N.D. Rago, J. Guo, T. Rojas, A.T. Ngo, K. Amine, Solvation-protection-enabled high-voltage electrolyte for lithium metal batteries, *Nano Energy* 92 (2022), 106720.
- [2] Z. Li, X. Huang, L. Kong, N. Qin, Z. Wang, L. Yin, Y. Li, Q. Gan, K. Liao, S. Gu, T. Zhang, H. Huang, L. Wang, G. Luo, X. Cheng, Z. Lu, Gradient nano-recipes to guide lithium deposition in a tunable reservoir for anode-free batteries, *Energy Storage Mater.* 45 (2022) 40–47.
- [3] P. Zhai, T. Wang, H. Jiang, J. Wan, Y. Wei, L. Wang, W. Liu, Q. Chen, W. Yang, Y. Cui, Y. Gong, 3D artificial solid-electrolyte interphase for lithium metal anodes enabled by insulator-metal-insulator layered heterostructures, *Adv. Mater.* 33 (13) (2021) 2006247.
- [4] Z. Huang, S. Choudhury, H. Gong, Y. Cui, Z. Bao, A cation-tethered flowable polymeric interface for enabling stable deposition of metallic lithium, *J. Am. Chem. Soc.* 142 (51) (2020) 21393–21403.
- [5] S.-J. Park, J.-Y. Hwang, Y.-K. Sun, Trimethylsilyl azide ($C_3H_9N_3Si$): a highly efficient additive for tailoring fluoroethylene carbonate (FEC) based electrolytes for Li-metal batteries, *J. Mater. Chem. A* 7 (22) (2019) 13441–13448.
- [6] K. Zhang, F. Wu, K. Zhang, S. Weng, X. Wang, M. Gao, Y. Sun, D. Cao, Y. Bai, H. Xu, X. Wang, C. Wu, Chlorinated dual-protective layers as interfacial stabilizer for dendrite-free lithium metal anode, *Energy Storage Mater.* 41 (2021) 485–494.
- [7] L. Ye, M. Liao, X. Cheng, X. Zhou, Y. Zhao, Y. Yang, C. Tang, H. Sun, Y. Gao, B. Wang, H. Peng, Lithium metal anodes working at 60 mA cm^2 and 60 mAh cm^2 through nanoscale lithium-ion adsorbing, *Angew. Chem. Int. Ed. Engl.* 133 (32) (2021) 17559–17565.
- [8] W. Xu, X. Liao, W. Xu, C. Sun, K. Zhao, Y. Zhao, C. Hu, Gradient SEI layer induced by liquid alloy electrolyte additive for high rate lithium metal battery, *Nano Energy* 88 (2021), 106237.
- [9] Z. Shen, W. Zhang, S. Mao, S. Li, X. Wang, Y. Lu, Tailored electrolytes enabling practical lithium-sulfur full batteries via interfacial protection, *ACS Energy Lett.* (2021) 2673–2681.
- [10] C.V. Amanchukwu, Z. Yu, X. Kong, J. Qin, Y. Cui, Z. Bao, A new class of ionically conducting fluorinated ether electrolytes with high electrochemical stability, *J. Am. Chem. Soc.* 142 (16) (2020) 7393–7403.
- [11] Y.H. Tan, G.X. Lu, J.H. Zheng, F. Zhou, M. Chen, T. Ma, L.L. Lu, Y.H. Song, Y. Guan, J. Wang, Z. Liang, W.S. Xu, Y. Zhang, X. Tao, H.B. Yao, Lithium fluoride in electrolyte for stable and safe lithium-metal batteries, *Adv. Mater.* 33 (42) (2021) 2102134.
- [12] G. Lu, J. Nai, H. Yuan, J. Wang, J. Zheng, Z. Ju, C. Jin, Y. Wang, T. Liu, Y. Liu, X. Tao, In-situ electrodeposition of nanostructured carbon strengthened interface for stabilizing lithium metal anode, *ACS Nano* 16 (6) (2022) 9883–9893.
- [13] K. Zhang, W. Liu, Y. Gao, X. Wang, Z. Chen, R. Ning, W. Yu, R. Li, L. Li, X. Li, K. Yuan, L. Ma, N. Li, C. Shen, W. Huang, K. Xie, K.P. Loh, A high-performance lithium metal battery with ion-selective nanofluidic transport in a conjugated microporous polymer protective layer, *Adv. Mater.* 33 (5) (2021) 2006323.
- [14] K. Yan, Z. Lu, H.-W. Lee, F. Xiong, P.-C. Hsu, Y. Li, J. Zhao, S. Chu, Y. Cui, Selective deposition and stable encapsulation of lithium through heterogeneous seeded growth, *Nat. Energy* 1 (3) (2016) 16010.
- [15] R. Saroha, J.S. Cho, Nanofibers comprising interconnected chain-like hollow N-doped C nanocages as 3D free-standing cathodes for Li-S batteries with super-high sulfur content and lean electrolyte/sulfur ratio, *Small Methods* 6 (5) (2022) 2200049.

- [16] Z.Y. Wang, Z.X. Lu, W. Guo, Q. Luo, Y.H. Yin, X.B. Liu, Y.S. Li, B.Y. Xia, Z.P. Wu, A dendrite-free lithium/carbon nanotube hybrid for lithium-metal batteries, *Adv. Mater.* 33 (4) (2021) 2006702.
- [17] J. Qian, W.A. Henderson, W. Xu, P. Bhattacharya, M. Engelhard, O. Borodin, J. G. Zhang, High rate and stable cycling of lithium metal anode, *Nat. Commun.* 6 (2015) 6362.
- [18] C. Zhu, C. Sun, R. Li, S. Weng, L. Fan, X. Wang, L. Chen, M. Noked, X. Fan, Anion-diluent pairing for stable high-energy Li metal batteries, *ACS Energy Lett.* 7 (4) (2022) 1338–1347.
- [19] X. Cao, P. Gao, X. Ren, L. Zou, M.H. Engelhard, B.E. Matthews, J. Hu, C. Niu, D. Liu, B.W. Arey, C. Wang, J. Xiao, J. Liu, W. Xu, J.G. Zhang, Effects of fluorinated solvents on electrolyte solvation structures and electrode/electrolyte interphases for lithium metal batteries, *Proc. Natl. Acad. Sci. U. S. A.* 118 (9) (2021) 2020357118.
- [20] J. You, H. Deng, X. Zheng, H. Yan, L. Deng, Y. Zhou, J. Li, M. Chen, Q. Wu, P. Zhang, H. Sun, J. Xu, Stabilized and almost dendrite-free Li metal anodes by in situ construction of a composite protective layer for Li metal batteries, *ACS Appl. Mater. Inter.* 14 (4) (2022) 5298–5307.
- [21] H. Zhang, J. Luo, M. Qi, S. Lin, Q. Dong, H. Li, N. Dulock, C. Povernelli, N. Wong, W. Fan, J.L. Bao, D. Wang, Enabling lithium metal anode in nonflammable phosphate electrolyte with electrochemically induced chemical reactions, *Angew. Chem. Int. Ed. Engl.* 60 (35) (2021) 19183–19190.
- [22] R. Xu, X. Shen, X.X. Ma, C. Yan, X.Q. Zhang, X. Chen, J.F. Ding, J.Q. Huang, Identifying the critical anion-cation coordination to regulate the electric double layer for an efficient lithium-metal anode interface, *Angew. Chem. Int. Ed. Engl.* 60 (8) (2021) 4215–4220.
- [23] H. Wang, Z. Yu, X. Kong, W. Huang, Z. Zhang, D.G. Mackanic, X. Huang, J. Qin, Z. Bao, Y. Cui, Dual-solvent Li-ion solvation enables high-performance Li-metal batteries, *Adv. Mater.* 33 (15) (2021) 2008619.
- [24] S. Zhu, J. Chen, Dual strategy with Li-ion solvation and solid electrolyte interphase for high Coulombic efficiency of lithium metal anode, *Energy Storage Mater.* 44 (2022) 48–56.
- [25] D. Xiao, Q. Li, D. Luo, R. Gao, Z. Li, M. Feng, T. Or, L. Shui, G. Zhou, X. Wang, Z. Chen, Establishing the preferential adsorption of anion-dominated solvation structures in the electrolytes for high-energy-density lithium metal batteries, *Adv. Funct. Mater.* 31 (30) (2021) 2011109.
- [26] Z. Wang, F. Qi, L. Yin, Y. Shi, C. Sun, B. An, H.M. Cheng, F. Li, An anion-tuned solid electrolyte interphase with fast ion transfer kinetics for stable lithium anodes, *Adv. Energy Mater.* 10 (14) (2020) 1903843.
- [27] J. Holoubek, H. Liu, Z. Wu, Y. Yin, X. Xing, G. Cai, S. Yu, H. Zhou, T.A. Pascal, Z. Chen, P. Liu, Tailoring electrolyte solvation for Li metal batteries cycled at ultra-low temperature, *Nat. Energy* 6 (2021) 303–313.
- [28] D. Wu, J. He, J. Liu, M. Wu, S. Qi, H. Wang, J. Huang, F. Li, D. Tang, J. Ma, $\text{Li}_2\text{CO}_3/\text{LiF}$ -rich heterostructured solid electrolyte interphase with superior lithiophilic and Li^+ -transferred characteristics via adjusting electrolyte additives, *Adv. Energy Mater.* 12 (18) (2022) 2200337.
- [29] M.S. Kim, Z. Zhang, P.E. Rudnicki, Z. Yu, J. Wang, H. Wang, S.T. Oyakhire, Y. Chen, S.C. Kim, W. Zhang, D.T. Boyle, X. Kong, R. Xu, Z. Huang, W. Huang, S.F. Bent, L.W. Wang, J. Qin, Z. Bao, Y. Cui, Suspension electrolyte with modified Li^+ solvation environment for lithium metal batteries, *Nat. Mater.* 21(4) (2022) 445–454.
- [30] H. Dai, K. Xi, X. Liu, C. Lai, S. Zhang, Cationic surfactant-based electrolyte additives for uniform lithium deposition via lithiophobic repulsion mechanisms, *J. Am. Chem. Soc.* 140(50) (2018) 17515–17521.
- [31] C.B. Jin, X.Q. Zhang, O.W. Sheng, S.Y. Sun, L.P. Hou, P. Shi, B.Q. Li, J.Q. Huang, X. Y. Tao, Q. Zhang, Reclaiming inactive lithium with a triiodide/iodide redox couple for practical lithium metal batteries, *Angew. Chem. Int. Ed. Engl.* 60 (42) (2021) 22990–22995.
- [32] Q. Zhao, Y. Lu, Z. Zhu, Z. Tao, J. Chen, Rechargeable lithium-iodine batteries with iodine/nanoporous carbon cathode, *Nano Lett.* 15 (9) (2015) 5982–5987.
- [33] J. Li, S. Liu, Y. Cui, S. Zhang, X. Wu, J. Xiang, M. Li, X. Wang, X. Xia, C. Gu, J. Tu, Potassium hexafluorophosphate additive enables stable lithium-sulfur batteries, *ACS Appl. Mater. Inter.* 12 (50) (2020) 56017–56026.
- [34] F. Ding, W. Xu, G.L. Graff, J. Zhang, M.L. Sushko, X. Chen, Y. Shao, M. H. Engelhard, Z. Nie, J. Xiao, X. Liu, P.V. Sushko, J. Liu, J.G. Zhang, Dendrite-free lithium deposition via self-healing electrostatic shield mechanism, *J. Am. Chem. Soc.* 135 (11) (2013) 4450–4456.
- [35] J. Yang, T. Feng, C. Zhi, J. Li, H. Zhou, C. Chen, Y. Song, M. Wu, Bimetallic composite induced ultra-stable solid electrolyte interphase for dendrite-free lithium metal anode, *J. Colloid Interfaces Sci.* 599 (2021) 819–827.
- [36] H. Yang, L. Yin, H. Shi, K. He, H.M. Cheng, F. Li, Suppressing lithium dendrite formation by slowing its desolvation kinetics, *Chem. Commun.* 55 (88) (2019).
- [37] Y. Qiao, S. Wu, Y. Sun, S. Guo, J. Yi, P. He, H. Zhou, Unraveling the complex role of iodide additives in Li-O_2 batteries, *ACS Energy Lett.* 2 (8) (2017) 1869–1878.
- [38] C. Jin, T. Liu, O. Sheng, M. Li, T. Liu, Y. Yuan, J. Nai, Z. Ju, W. Zhang, Y. Liu, Y. Wang, Z. Lin, J. Lu, X. Tao, Rejuvenating dead lithium supply in lithium metal anodes by iodine redox, *Nat. Energy* 6 (4) (2021) 378–387.
- [39] G. Wang, X. Xiong, D. Xie, X. Fu, X. Ma, Y. Li, Y. Liu, Z. Lin, C. Yang, M. Liu, Suppressing dendrite growth by a functional electrolyte additive for robust Li metal anodes, *Energy Storage Mater.* 23 (2019) 701–706.
- [40] H. Sun, J. Liu, J. He, H. Wang, G. Jiang, S. Qi, J. Ma, Stabilizing the cycling stability of rechargeable lithium metal batteries with tris(hexafluoroisopropyl) phosphate additive, *Sci. Bull.* 67 (7) (2022) 725–732.
- [41] Q. Yang, J. Hu, J. Meng, C. Li, C-F-rich oil drop as non-expendable fluid interface modifier with low surface energy to stabilize Li metal anode, *Energy Environ. Sci.* 14 (2021) 3621–3631.
- [42] F. Li, J. He, J. Liu, M. Wu, Y. Hou, H. Wang, S. Qi, Q. Liu, J. Hu, J. Ma, Gradient solid electrolyte interphase and lithium-ion solvation regulated by bisfluoroacetamide for stable lithium metal batteries, *Angew. Chem. Int. Ed. Engl.* 60 (12) (2021) 6600–6608.